Revista Mexicana de Astronomía y Astrofísica Serie de Conferencias (RMxAC), **59**, 63–68 (2025)

https://doi.org/10.22201/ia.14052059p.2025.59.12

VII Workshop on Robotic Autonomous Observatories (October 16-20, 2023)
Editors: Maria Gritsevich, Alberto J. Castro-Tirado, Petr Kubánek, Shashi B. Pandey, and David Hiriart - DOI: https://doi.org/10.22201/ia.14052059p.2025.59.12

SKY BRIGHTNESS MEASUREMENTS WITH THE ALLSKY CAMERA AT THE UNIVERSITY OF GÖTTINGEN

K. J. Schimpf[1] and T. O. Husser [2]

RESUMEN

El telescopio de 50 cm utilizado por el Instituto de Astrofísica y Geofísica (IAG) de la Universidad de Göttingen está ubicado en la azotea de la Facultad de Física en las afueras de la ciudad. Esto significa que las ventanas de observación disponibles no sólo están limitados por la nubosidad, sino también por la contaminación lumínica provocada por la ciudad, lo que también afecta a la calidad de las mediciones. Al ampliar las capacidades de nuestro sistema de control de telescopios 'pyobs', este proyecto implementará una medición en tiempo real del brillo del cielo y la cobertura de nubes, brindando la capacidad de seleccionar los objetos a ser observados de acuerdo con estas mediciones. Se creará un módulo de control de cámara Allsky, 'pyobs-allsky', que gestionará el tiempo de exposición y la configuración de ganancia, y utilizará un canal de reducción de las imágenes y las coincidencias con los catálogos para así poder cumplir con los requisitos.

ABSTRACT

The 50-cm telescope used by the Institute for Astrophysics and Geophysics (IAG) at the University of Göttingen is located on the roof of the physics faculty on the outskirts of the city. This means that the available observing targets are not only limited by cloud cover, but also by the light pollution caused by the city, which also affects the quality of the measurements. By extending the capabilities of our telescope control system 'pyobs', this project will implement a real-time measurement of sky brightness and cloud cover, providing the ability to select observation targets according to these measurements. An Allsky camera control module 'pyobs-allsky' will be created, which will manage the exposure time and gain settings, and will use an image reduction pipeline and catalogue matching to meet the requirements.

Key Words: Allsky camera — Sky brightness — Cloud detection — pyobs

1. INTRODUCTION

Robotic telescopes and automatic target scheduling are considered solved problems; predicting target visibility is one of the next frontiers for optimising observing time. While remote observation locations with dry climates face target altitude as the primary limiting factor for visibility, urban European observation sites must also factor in cloud coverage and light pollution from nearby towns and cities when planning observations. The Institute for Astrophysics and Geophysics (IAG) operates a fully robotic 50 cm Cassegrain telescope on the roof of the institute using the observation control system pyobs[3] (Husser et al. 2022a,b). With only a few photometric nights per year and significant light pollution from the town of Göttingen, it is a good example of the challenging telescope sites described above. Next to the telescope is a suite of weather sensors, already used by the pyobs-weather[4] weather control system. These are complemented by an allsky camera, which is currently only used for manual weather confirmation. Automated analysis of the allsky images, together with the existing weather data, should enable spatially resolved sky brightness measurements and cloud detection, as well as prediction of cloud cover for short time periods. This paper presents the preliminary results of this analysis.

2. METHODS

The data collection process is described by two layers. The physical hardware used to measure the weather at IAG and the software responsible for managing and analysing the obtained weather data.

2.1. *Sensors*

As described above, the sensors are located next to the 50 cm telescope on the roof of the Faculty of Physics building. A Boltwood III cloud sensor is mainly used for sky temperature measurements and

[1]Institute for Astrophysics and Geophysics, University of Göttingen, Friedrich-Hund-Platz 1, 37077 Göttingen, GER, (k.schimpf@stud.uni-goettingen.de).

[2]Institute for Astrophysics and Geophysics, University of Göttingen, Friedrich-Hund-Platz 1, 37077 Göttingen, GER, (thusser@uni-goettingen.de).

[3]`https://pyobs.org`

[4]`https://github.com/pyobs/pyobs-weather`

VII Workshop on Robotic Autonomous Observatories (October 16-20, 2023)
Editors: Maria Gritsevich, Alberto J. Castro-Tirado, Petr Kubánek, Shashi B. Pandey, and David Hiriart - DOI: https://doi.org/10.22201/ia.14052059p.2025.59.12

rain detection. The sky temperature is determined by measuring the surface brightness of the zenith in an infrared band. Similarly, a Sky Quality Meter (SQM) measures the surface brightness of the zenith in the visible band, resulting in a measurement of sky brightness. Both sensors cannot spatially resolve the sky. In addition, a weather station measures temperature, humidity, wind direction and speed. The allsky camera, a ASI 120 MC-S Color from ZWO, is located next to the other sensors. It has a field of view of 150, allowing it to capture most of the sky. To allow better control of exposure times, it operates at a cadence of 1 frame per minute. To prevent dew formation on the camera housing, the housing is heated by a 12 W heating element. As the dew point temperature in Göttingen does not exceed 15 °C, the heater is only switched on when the temperature inside the housing falls below 15 °C. An 80 mm cooling fan is used above 40 °C to reduce the risk of overheating in summer.

2.2. *Software Architecture*

The architecture connecting all the sensors mentioned above follows the micro-service architecture also used by pyobs. The pyobs-allsky module controls a pyobs camera module to which it is connected via pyobs. While the pyobs camera module only provides an interface for the allsky camera, the pyobs-allsky module is responsible for exposure time control, imaging cadence and file output. The file output includes the raw fits image and a compressed version with an overlay to be used on the Institute's public website. These files are then hosted by a static file server so that they can be accessed remotely. The weather sensor data is aggregated by the pyobs-weather module and stored in a time series database (InfluxDB). The current and historical weather data can be retrieved via a A REpresentational State Transfer Application Programming Interface (REST API) provided by the pyobs-weather module. The allsky-analyser module, currently under development, will access both the weather API and raw allsky imagery to compute the current sky brightness and cloud map, and to predict cloud movement. This will then be used to provide a REST API for checking current and future target visibility.

3. RESULTS

First, a relationship between the celestial and image coordinates is established by fitting a World Coordinate System (WCS). This is subsequently used to determine the visibility of catalogue stars in an

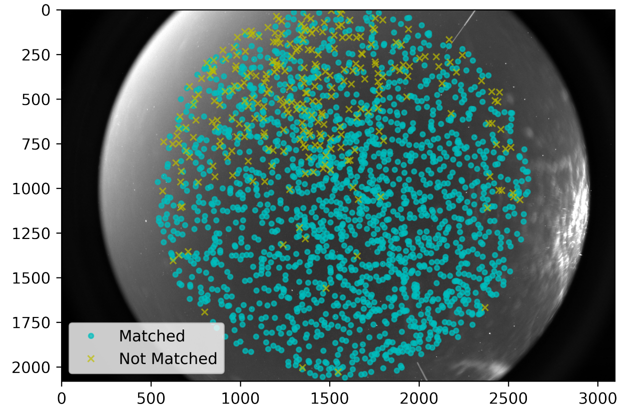

Fig. 1. Allsky image of a clear sky. Matched and not matched stars are marked with circles and crosses respectively for ALT > 30°.

image. Sorting the visible and invisible stars around each pixel by visual magnitude and calculating the limiting magnitude between these groups produces a limiting magnitude map. Subtracting the map for the ideal scenario, where all stars are visible, results in a map that showcases the change in limiting magnitude compared to a perfectly clear sky. Assuming that clouds are causing this change, the map corresponds to the cloud cover. A sky brightness map is derived from the limiting magnitude map using the linear relationship between limiting magnitude and sky brightness and the sky brightness data collected by the SQM. Furthermore, the sky brightness data obtained from the SQM is correlated with the sky temperature measurements of the Boltwood III sensor to explore the potential substitution of a sky temperature sensor with a sky brightness sensor.

3.1. *World Coordinate System (WCS)*

In order to relate pixel positions in the image to celestial coordinates, it is required to define a World Coordinate System (WCS). For the allsky camera, an hour angle-declination model has been adopted, with an Airy projection and a simple imaging polynomial (SIP) of third degree. A list of coordinate pairs is required to fit this model, but since a WCS is crucial to find these pairs, multiple iterations are required to determine the final WCS. The stars in each image are identified using using the Python library for Source Extraction and Photometry (SEP) (Bertin & Arnouts 1996; Barbary 2016). Then, in the initial iteration, a limited number of bright stars are matched with their respective catalogue counterparts manually. This minimal set of pairs is adequate for fitting a basic astrometric model for the allsky camera (Barghini et al. 2019). In the second

VII Workshop on Robotic Autonomous Observatories (October 16-20, 2023)
Editors: Maria Gritsevich, Alberto J. Castro-Tirado, Petr Kubánek, Shashi B. Pandey, and David Hiriart - DOI: https://doi.org/10.22201/ia.14052059p.2025.59.12

iteration, the simplified model is employed to match all stars found in all images of a photometric night to increase the number of pairs. These are then used to fit the WCS model. The fit results in a root mean square error of 3.10 pixels on the x-axis and 3.06 pixels on the y-axis in the image, and 11.81' in altitude and 17.48' in azimuth in the sky.

3.2. *Reverse matching*

The next objective is to determine if a catalogue star is visible in an image $I(v, w)$, which pixels can be indexed by the pixel coordinates (v, w). Using the WCS described in § 3.1, the stars are projected onto the image in the sky, resulting in pixel coordinates (x, y). These coordinates then define a window area

$$W_I[i] : [0..2i+1]^2 \to \mathbb{N},$$
$$W_I[i](a, b) = I(x - i + a, y - i + b),$$

where $2i + 1$ is the length of one side of the area. A catalogue star is found in the image if a significant peak is found in the window area, so

$$\exists a, b \in [0..2i+1]^2 : W[i](a, b) \geq \overline{W} + 3\sigma,$$

where $\overline{W}$ is the mean of the window and σ is the standard deviation of that mean. Applying this to all stars in the catalogue that are above the horizon at the time the image was taken will give a list of visible and invisible stars in the image. Figure 1 shows the resulting matches for a clear and cloudy sky for stars with ALT $> 30°$. For the cloudy sky the invisible stars match well with the visible clouds, while for the clear sky they match up with the areas of high sky brightness.

3.3. *Limiting magnitude map*

The limiting visual magnitude can be determined using the lists of visible and invisible stars in the image from § 3.2. For a pixel position (x, y) in the image, both lists are filtered for stars that are within a distance R of the pixel position. Ordering these stars by their visual magnitude gives four cases for the resulting lists, as can be seen in Figure 3. The limiting magnitude can be calculated for these cases using the following algorithm:

1. If all stars are visible, the limiting visual magnitude is assumed to be equal to the highest magnitude star in the list.

2. If all stars are invisible, the limiting magnitude is assumed to be equal to the lowest magnitude star in the list.

3. If all the invisible stars are of lower magnitude than the visible stars, the limiting magnitude is assumed to be the average of the magnitude of the lowest visible star and the highest invisible star. The stars are weighted by their distance from the pixel position.

4. If there are invisible stars with magnitudes greater than the visible stars, the limiting magnitude is assumed to be the average magnitude of all the invisible stars with magnitudes greater than the lowest visible star, and vice versa. The stars are weighted according to their distance from the position of the pixel.

For the last two cases, this also gives an estimated error in the form of the standard deviation of the averages. Applying this to all the pixels in the image produces a map of the limiting magnitude, accompanied by an error map, displayed in Figure 2. As expected from the algorithm, regions of low visual magnitude and high standard deviation correspond to regions with many invisible stars.

3.4. *Cloud map*

Assuming that limiting visual magnitude is solely influenced by cloud coverage and all stars in the catalogue are visible during clear skies, a cloud coverage map may be generated by subtracting the limiting magnitude map acquired in § 3.3 from the corresponding map that represents the situation where all stars are visible. The resulting map will express the change in visible magnitude with respect to the ideal case. A threshold value can be determined to discern when a difference in visual magnitude signifies a cloud. Overlaying this image using a threshold of 0.5 generates Figure 4a. Figure 4b shows the same image, but with marked invisible stars. Comparing Figure 4a to Figure 4b, indicates that the detected clouds are mostly consistent with the visible clouds where the catalogue has a high enough star density. The large chosen radius R, in which the visibility of stars is still taken into account for a given pixel, results in insufficient spatial resolution of the clouds. Also Figure 1 shows invisible stars for a clear sky, which means, that the assumption of all stars being visible for a clear sky is violated.

3.5. *Sky brightness map*

The relation between the limiting magnitude m_0 and the sky surface brightness μ can be described by a linear function (Crumey 2014). The measured limiting magnitude in § 3.3 is limited by the camera optics and the star catalogue used to match the stars,

VII Workshop on Robotic Autonomous Observatories (October 16-20, 2023)
Editors: Maria Gritsevich, Alberto J. Castro-Tirado, Petr Kubánek, Shashi B. Pandey, and David Hiriart - DOI: https://doi.org/10.22201/ia.14052059p.2025.59.12

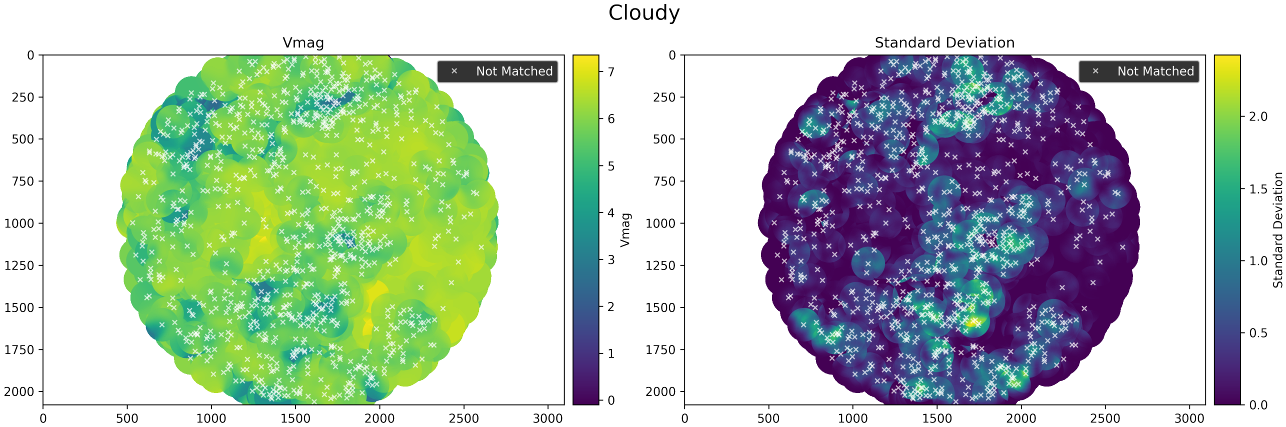

Fig. 2. Limiting visual magnitude map (left) and standard deviation (right) generated from a cloudy allsky image. In both plots crosses mark not matched stars.

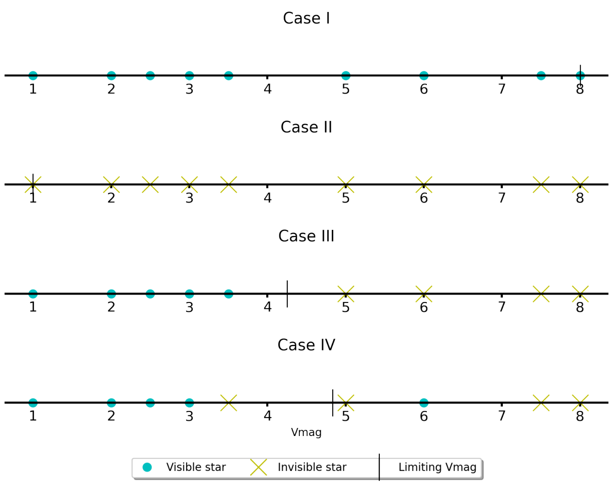

Fig. 3. Four examples of calculating the limiting magnitude from a group of nearby stars. The visual magnitude for the stars and the calculated limiting visual magnitude are shown.

which implies a maximum limiting magnitude above a limiting sky brightness μ_{limit}. This yield the fit function

$$m_0(\mu) = \begin{cases} a \cdot \mu + b & x \leq \mu_{\text{limit}} \\ a \cdot \mu_{\text{limit}} + b & x \geq \mu_{\text{limit}} \end{cases}, \tag{1}$$

where a, b are free fit parameters. The free parameters are found by fitting this function with the surface brightness measurements made by the SQM described in § 2.1 and the limiting magnitude found by the algorithm described in § 3.3. Using the data of one night to fit this function results in $a = (1.523 \pm 0.006)\,\text{arcsec}^2$, $b = (-22.7 \pm 1.3)\,\text{mag}$ and $\mu_{\text{limit}} = (19.08 \pm 0.07)\,\text{mag/arcsec}^2$. Figure 5 illustrates the data for the fitted night and function. It can be seen that the function fits the data well, but also that measurements were made with $\mu > \mu_{\text{limit}}$. This means that using this configuration only a sky brightness below $\mu_{\text{limit}} = (19.08 \pm 0.07)\,\text{mag/arcsec}^2$ can be measured correctly.

3.6. *Sky brightness and temperature*

The IAG currently operates a Boltwood sensor for cloud detection. This is described in § 2.1. However, a comparison of the Boltwood sensor with the SQM shows that both sensors effectively measure the surface brightness of the zenith, but at different wavelengths and price ranges: While the SQM measures brightness in the range $300 - 1100\,\text{nm}$, the Boltwood sensor operates in the range $8 - 15\,\mu\text{m}$, but costs about ten times as much. This leads to the question of whether the SQM could be a more economical alternative to the Boltwood sensor for cloud detection. Figure 6 shows both the sky temperature measured by the Boltwood sensor and the sky brightness measured by the SQM over a period of one night. The figures shows some correlation between the sensors, but it is noticeable that in the darkest conditions the sky brightness lacks features that are visible in the sky temperature. Plotting sky brightness against sky temperature for one month, as shown in Figure 7, also suggests this imperfect correlation. This can be quantified by the Pearson r-value $r = -0.81$ with a p-value $p = 0.0$, which also supports the suggestion.

4. DISCUSSION

The WCS presented in § 3.1 provides sufficient accuracy above ALT $> 30°$ for the reverse matching algorithm shown in § 3.2. By visual inspection, the results of the reverse matching algorithm appear to match the actual visibility of the stars. The algorithm used to compute the limiting magnitude map

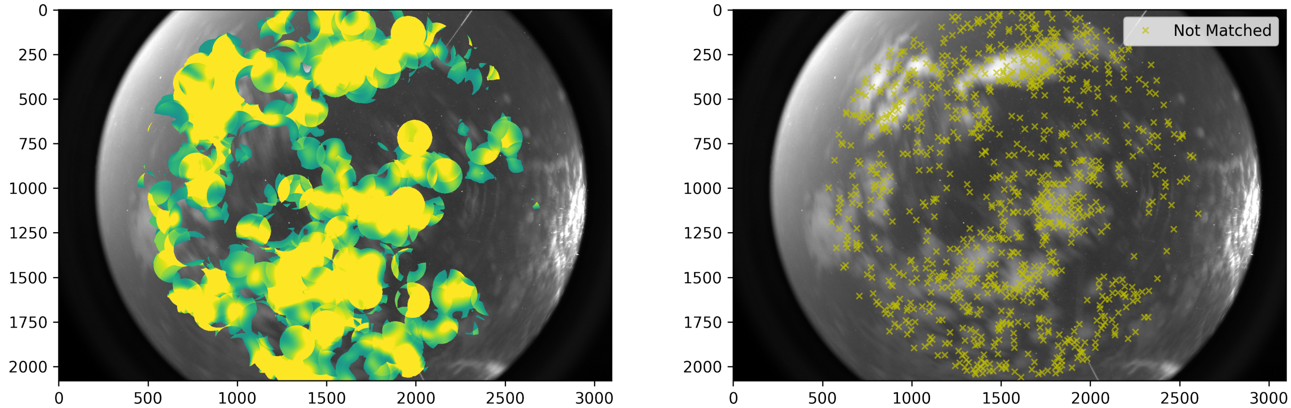

Fig. 4. Comparison between the cloud map on the left and the allsky image with the not matched stars. The cloud map is superimposed on the Allsky image, while values < 0.5 have been made transparent in the cloud map.

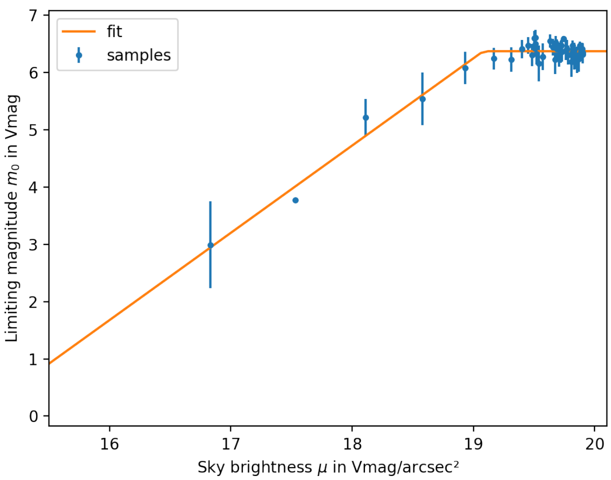

Fig. 5. The limiting visual magnitude at the zenith calculated in § 3.3 plotted against the sky brightness measured by the SQM for one evening. The data are fitted with the linear relation described by Equation 1.

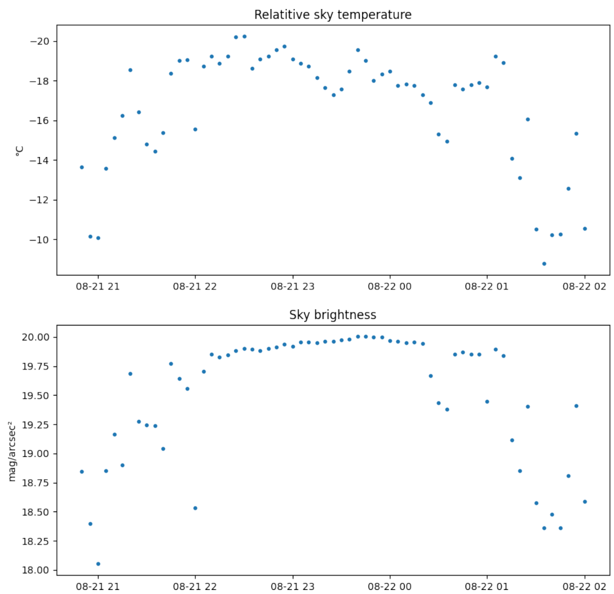

Fig. 6. Relative sky temperature measured with the Boltwood III and sky brightness measured with the SQM for one night with samples every 5 minutes.

described in § 3.3 produces plausible results, but when used to compute the sky magnitude it fails to reproduce the sky magnitude measured by the SQM. This is probably due to the limited magnitude of the catalogue used for the reverse matching or the limited exposure time of the allsky camera. In addition, the algorithm only approximates the limiting magnitude, as the catalogue visual magnitude used differs from the actual apparent magnitude of the stars due to air mass and star type. Using the limiting magnitude map for cloud detection by subtracting the limiting magnitude map for a perfect sky in § 3.4 also gives useful results. However, the clear sky image in Figure 1 shows that the assumption of a perfect sky does not correspond to the clear sky found in Göttingen, as not all stars are detected. This could be solved by taking the light pollution into account, when generating the cloudless map. That would also require accounting for time variable source as the sun and moon. The cloud map is also poorly spatially resolved because the radius used to group stars for the limiting magnitude map generation algorithm needs to be large enough to include enough stars. Using a continuous star visibility instead of the binary might alleviate this problem by providing more information per star. Determining the star visibility using a Laplacian of Gaussian filter (Adam et al. 2017) or point source photometry could be possible solutions. The sky brightness and sky temperature analysed in § 3.6 show a clear correlation. Whether this is sufficient to replace a sky temperature sensor with a sky

VII Workshop on Robotic Autonomous Observatories (October 16-20, 2023)
Editors: Maria Gritsevich, Alberto J. Castro-Tirado, Petr Kubánek, Shashi B. Pandey, and David Hiriart - DOI: https://doi.org/10.22201/ia.14052059p.2025.59.12

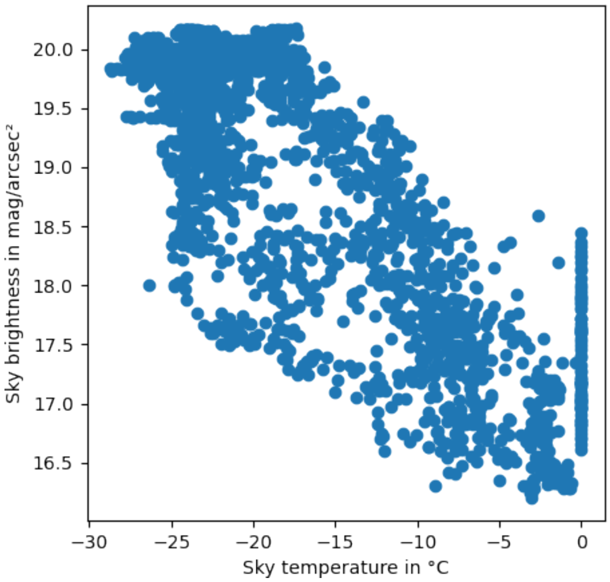

Fig. 7. Sky brightness measured with the SQM plotted against relative sky temperature measured with the Boltwood III for one month. The data is filtered for solar altitudes below $< -18°$.

quality meter needs further investigation. In the future, a cloud tracking system will be implemented by utilising a clustering algorithm, as previously demonstrated by Adam et al. 2017. Measuring the cloud height with the allsky camera (Jechow et al. 2019) and using the wind speed and direction data from our weather station would then allow for better prediction of cloud movement.

5. CONCLUSION AND SUMMARY

We presented the operational setup of the allsky camera and weather sensor at the IAG. The data gathering and hardware components of the project are functional, although the analysis module is still in the prototyping phase. We demonstrated an initial attempt to estimate star visibility and produce maps of sky brightness and cloud coverage using, at present, solely binary star visibility. However, the resulting maps are limited to ALT $> 30°$ and not spatially well-resolved. This must be addressed to enhance accuracy and monitor clouds over multiple images. We examined the potential estimation of sky temperature based on sky brightness measurements, and while a clear correlation is evident, further research is necessary to apply this method. In conclusion we showed that external weather sensors can be used to improve allsky image analysis.

REFERENCES

Adam, J., Buss, J., Brügge, K., et al. 2017, EPJWC, 144, 01004, doi:10.1051/epjconf/201714401004

Barbary, K. 2016, asci.soft, 1, 58, doi:10.21105/joss.00058

Barghini, D., Gardiol, D., Carbognani, A., et al. 2019, A&A, 626, A105, doi:10.1051/0004-6361/201935580

Bertin, E. & Arnouts, S. 1996, A&AS, 117, 393, doi:10.1051/aas:1996164

Crumey, A. 2014, MNRAS, 442, 2600, doi:10.1093/mnras/stu992

Husser, T.-O., Hessman, F. V., Martens, S., et al. 2022, FrASS, 9, 891486, doi:10.3389/fspas.2022.891486

Husser, T.-O., Hessman, F. V., Martens, S., et al. 2022, Astrophysics Source Code Library, ascl:2203.012

Jechow, A., Hölker, F., & Kyba, C. C. M. 2019, NatSR, 9, 1391, doi:10.1038/s41598-018-37817-8